GEOPHYSICS, VOL. 75, NO. 3 (MAY-JUNE 2010); P. D13–D26, 15 FIGS., 1 TABLE.
10.1190/1.3431045

2D and 3D elastic wavefield vector decomposition in the wavenumber domain for VTI media

Qunshan Zhang[1] and George A. McMechan[1]

ABSTRACT

A pragmatic decomposition of a vector wavefield into P- and S-waves is based on the Helmholtz theory and the Christoffel equation. It is applicable to VTI media when the plane-wave polarization is continuous in the vicinity of a given wavenumber and is uniquely defined by that wavenumber, except for the kiss singularities on the VTI symmetry axis. Unlike divergence and curl, which separate the wavefield into a scalar and a vector field, the decomposed P- and S-wavefields are both vector fields, with correct amplitude, phase, and physical units. If the vector components of decomposed wavefields are added, they reconstruct those of the original input wavefield. Wavefield propagation in any portions of a VTI medium that have the same polarization distribution (i.e., the same eigenvector) in the wavenumber domain have the same decomposition operators and can be reconstructed with a single 3D Fourier transform for each operator (e.g., one for P-waves and one for S-waves).This applies to isotropic wavefields and to VTI anisotropic wavefields, if the polarization distribution is constant, regardless of changes in the velocity. Because the anisotropic phase polarization is local, not global, the wavefield decomposition for inhomogeneous anisotropic media needs to be done separately for each region that has a different polarization distribution. The complete decomposed vector wavefield is constructed by combining the P-, SV-, and SH-wavefields in each region into the corresponding composite P-, SV-, and SH-wavefields that span the model. Potential practical applications include extraction of separate images for different wave types in prestack reverse time migration, inversion, or migration velocity analysis, and calculation of wave-propagation directions for common-angle gathers.

INTRODUCTION

Elastic (including anisotropic) wave propagation has been widely studied. Three-dimensional, three-component (3-C) reverse time extrapolation from 3-C receiver arrays will reconstruct both the P- and S-waves. Without P- and S-wave separation, the P and S converted waves will coincide in space and time at the image condition in reverse time migration. This superposition corrupts the migrated image; the image amplitudes have no physical meaning. Thus, the P- and S-wavefields need to be decomposed to allow isolation of P and S images (e.g., Sun et al., 2007; Yan and Sava, 2007).

Many authors have worked on P-S wavefield separation. The classical Helmholtz decomposition (Morse and Feshback, 1953) defines vector decomposition via calculating potentials, but this is applicable only for isotropic media and is too expensive to be practical. Devaney and Oristaglio (1986) separate the P- and S-waves by plane-wave decomposition. Amundsen and Reitan (1995) and Amundsen et al. (1998) separate the upgoing and downgoing P- and S-waves from the pressure and vector recorded data. Ma and Zhu (2003) extrapolate P- and S-waves separately in an elastic wavefield by decomposing the wave equation into P- and S-wave components. Jianlei et al. (2007) implement the Ma and Zhu (2003) algorithm with 2D staggered-grid finite differences.

Sun and McMechan (2001) and Sun et al. (2006) use 3D divergence and curl to separate P- and S-waves for reverse time migration. A phase shift is introduced by curl or curllike separations and divergence or divergencelike separations (Sun et al., 2001) so that the waveforms are changed. More important, the physical meanings of the original variables are lost in these operations. Therefore, for example, we then cannot use the upgoing over downgoing amplitude ratio as the image condition to obtain images of the PP, SS, PS, and SP reflection coefficients by reverse time migration. Below, we provide a solution to this problem.

Dellinger and Etgen (1990) generalize divergence and curl to anisotropic media by constructing the operators in the wavenumber domain, independently solving the Christoffel equation at each

Manuscript received by the Editor 12 May 2009; revised manuscript received 30 November 2009; published online 17 June 2010.
[1]University of Texas at Dallas, Center for Lithospheric Studies, Richardson, Texas, U.S.A. E-mail: qxz035000@utdallas.edu; mcmec@utdallas.edu.

wavenumber of the wave propagation. We call these curllike and divergencelike separation operations. In anisotropic media, eigenvalues of the Christoffel equation are used to define phase velocities. S1 and S2 are the fast and slow S-waves, but these do not correspond to consistent (SV and SH) polarizations as a function of the propagation direction (or wavenumber) (Figures 1 and 2). This is one reason why there are many statements in the literature about the impossibility of separating the two S-waves (Dellinger, 1991). Crossover discontinuities occur only if the fast or slow phase velocities are followed, not if the polarizations are followed; kiss singularities occur along the vertical (K_z) wavenumber (Crampin and Yedlin, 1981; Vavryčuk, 2003). The nomenclature of SV and SH applies only to TI media. The key concept of decomposition is based on polarization rather than phase velocities (Crampin, 1981; Tsvankin, 1997).

In this paper, we develop and implement a new wavefield decomposition to separate the elastic wavefield into curl-free (P-wave) and divergence-free (S-wave) parts while preserving the original physical units, phase, amplitude, and vector characteristics of the data. We generalize wavefield decomposition in isotropic media to anisotropic media by using the eigenvectors of the Christoffel equation (Dellinger and Etgen, 1990) to replace P-wave polarization. In the wavenumber domain, P, SV, and SH can be obtained by projecting the 3D Fourier-transformed input wavefield onto the vector components of their polarization directions. In addition, SV and SH can also be obtained by two sequential cross products of the corresponding polarizations with the S-wavefield.

In VTI media, the S-waves have two types of singularity: crossovers and kisses. We can handle crossovers by using continuity of polarization, but we do not attempt to solve the kiss singularity problem (which has no known solution). We also extend this method to inhomogeneous anisotropic wavefield decomposition using the fact that anisotropic phase polarization is local, not global (Nistala and McMechan, 2005). We use only VTI media as examples.

The strategy of this paper is to combine two previously existing concepts with a new, integrated framework. Together, they provide a complete new solution to the problem of decomposition of an elastic wavefield into P- and S-waves for isotropic media, and they also provide new insights into decomposition in anisotropic media. The first existing basis is the Helmholtz theory (Morse and Feshbach, 1953), which relates P- and S-waves to their scalar and vector potentials for isotropic media. The second basis is the work by Dellinger and Etgen (1989, 1990) and Dellinger (1991), which opened the door for application to anisotropic media via the Christoffel equation.

A key distinction must be made between the concepts of wave separation (or transformation) and wave decomposition. *Wave separation* refers to isolation of P- and S-waves, usually in the form of divergencelike and curllike operations. The separated waves do not have the same waveform or magnitude as the input wavefield (there is a 90° phase shift [Dellinger, 1991; Sun et al., 2004]). More important, divergence is a scalar and curl is a vector with a different (orthogonal) direction from that of the input vector wavefield. The outputs of the proposed wavefield decomposition have the advantage that they are vector components that have the same amplitude, phase, waveform, direction, and physical units as the input wavefield. The sum of the decomposed vector components of the P- and S-waves reconstructs the original three-component wavefield (which is not true for previous separations). Separation of wave-

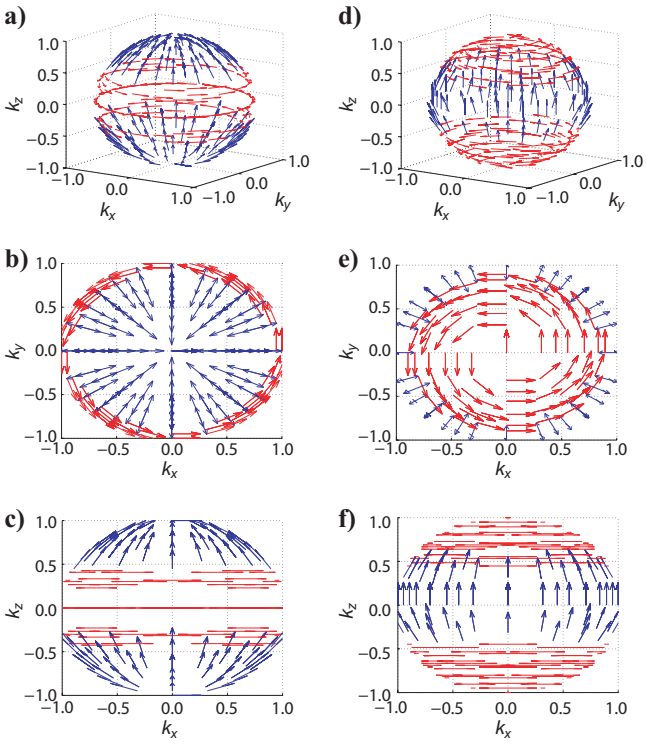

Figure 1. (a,b,c) The arrows show the S1 polarization directions at each **K** location. In (d,e,f,) they show the S2 polarization directions. $|\mathbf{K}| = 1.0$ and defines the wave-propagation direction. The blue arrows are SV; the red are SH. In (b and e), the arrows are projected to the horizontal (k_x,k_y) plane, and in (c and f) to the vertical (k_x,k_z) plane. Because k_z is a symmetry axis, the (k_y,k_z) plane is the same as the (k_x,k_z) plane and thus is not shown. The S1 and S2 patterns are complementary. The corresponding decompositions into SV and SH are shown in Figure 2.

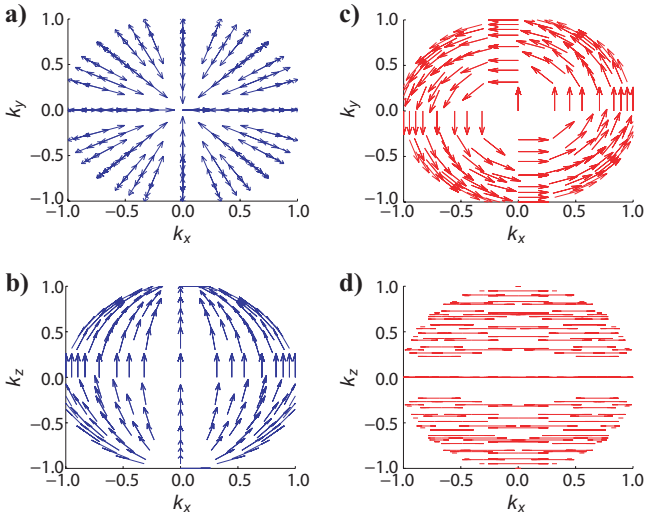

Figure 2. In (a) and (b), the arrows show the (predominantly longitudinal) SV polarization directions in the (k_x,k_y) and (k_x,k_z) projections, respectively; (c) and (d) are the same projections for the (transverse) SH polarization directions. The axes, symmetry, and color scheme are the same as in Figure 1, which shows the corresponding S1 and S2 representations. The use of SV and SH defined by polarization gives continuous polarization surfaces (except at the kiss singularities at $K_z = \pm 1$).

fields allows their use in image conditions for migration and reduces artifacts associated with P-S cross talk (Yan and Sava, 2007).

The main differences between the previous work and the current results are:

- Our derivation is mathematically rather than geometrically based. Thus, a side benefit is that the new derivation provides theoretical support for the work of Dellinger and Etgen (1990), Dellinger (1991), and Sun et al. (2004).
- Our outputs are the full 3-C vector wavefield decompositions (not transformations of the input wavefield).
- Our implementation and examples include 3D heterogeneous models, not just homogeneous models.
- We provide a physical interpretation of the full vector decomposition.

We provide a pragmatic approach to wavefield decomposition. Because the output consists of the vector components of each wave type, wave-incident directions are obtained very easily (and are necessary for AVA analysis). Thus, common-image gathers can be obtained directly in the angle domain without the need for space shifting in the crosscorrelation image condition. Space shifting is detailed by Sava and Fomel (2005).

THEORY

In this section, we consider the proposed formulation first in the isotropic context and then in the anisotropic context. Numerical examples are shown in the following section.

Wavefield decomposition in isotropic media

A 3D vector wavefield $\mathbf{U}$ can be expressed as

$$\mathbf{U} = U_x\mathbf{i} + U_y\mathbf{j} + U_z\mathbf{k}, \tag{1}$$

where $\mathbf{i}$, $\mathbf{j}$, and $\mathbf{k}$ are the unit basis vectors in a Cartesian-(x, y, z)-coordinate system, and U_x, U_y, and U_z are the wavefield components in the x-, y-, and z-directions, respectively. From the Helmholtz decomposition theory, a vector wavefield $\mathbf{U}$ can be decomposed into a curl-free part, $\mathbf{U}^{\mathrm{P}}$ (the P-wavefield), and a divergence-free part, $\mathbf{U}^{\mathrm{S}}$ (the S-wavefield) (Aki and Richards, 1980):

$$\mathbf{U} = \mathbf{U}^{\mathrm{P}} + \mathbf{U}^{\mathrm{S}}, \tag{2}$$

with

$$\nabla \times \mathbf{U}^{\mathrm{P}} = 0, \tag{3}$$

and

$$\nabla \cdot \mathbf{U}^{\mathrm{S}} = 0, \tag{4}$$

where

$$\nabla = \frac{\partial}{\partial x}\mathbf{i} + \frac{\partial}{\partial \mathbf{y}}\mathbf{j} + \frac{\partial}{\partial \mathbf{z}}\mathbf{k}.$$

The component forms of the curl-free (P-wave) part and the divergence-free (S-wave) part are

$$\mathbf{U}^{\mathrm{P}} = U_x^{\mathrm{P}}\mathbf{i} + U_y^{\mathrm{P}}\mathbf{j} + U_z^{\mathrm{P}}\mathbf{k}, \tag{5}$$

and

$$\mathbf{U}^{\mathrm{S}} = U_x^{\mathrm{S}}\mathbf{i} + U_y^{\mathrm{S}}\mathbf{j} + U_z^{\mathrm{S}}\mathbf{k}. \tag{6}$$

In the wavenumber domain, equation 1 is transformed to

$$\tilde{\mathbf{U}} = \tilde{U}_x\mathbf{i} + \tilde{U}_y\mathbf{j} + \tilde{U}_z\mathbf{k}. \tag{7}$$

The kernel of the Fourier transform is $e^{i(\mathbf{K}'\cdot\mathbf{R})}$, where $\mathbf{R} = (x,y,z)$ and $\mathbf{K}' = (K'_x,K'_y,K'_z)$ is the wavenumber vector that defines the wave-propagation (or P-wave-polarization) direction, and $K'_a = \omega/V_a$, where V_a is the phase velocity in direction a, ω is angular frequency, and $i = \sqrt{-1}$.

The Helmholtz equations are transformed into

$$\tilde{\mathbf{U}} = \tilde{\mathbf{U}}^{\mathrm{P}} + \tilde{\mathbf{U}}^{\mathrm{S}} \tag{8}$$

in the wavenumber domain, with

$$\mathbf{K}' \times \tilde{\mathbf{U}}^{\mathrm{P}} = 0 \tag{9}$$

and

$$\mathbf{K}' \cdot \tilde{\mathbf{U}}^{\mathrm{S}} = 0, \tag{10}$$

where the tilde on the wavefield variable indicates its 3D Fourier transform. Equations 8–10 correspond to equations 2–4, respectively. In addition, for a P-wave, we have

$$\nabla \cdot \mathbf{U} = \nabla \cdot \mathbf{U}^{\mathrm{P}} \tag{11}$$

in the space domain and

$$\mathbf{K}' \cdot \tilde{\mathbf{U}} = \mathbf{K}' \cdot \tilde{\mathbf{U}}^{\mathrm{P}} \tag{12}$$

in the wavenumber domain. Similarly, for an S-wave, we have

$$\nabla \times \mathbf{U} = \nabla \times \mathbf{U}^{\mathrm{S}} \tag{13}$$

in the space domain and

$$\mathbf{K}' \times \tilde{\mathbf{U}} = \mathbf{K}' \times \tilde{\mathbf{U}}^{\mathrm{S}} \tag{14}$$

in the wavenumber domain.

Consider solving for the Fourier vector components $\tilde{U}_x^{\mathrm{P}}$, $\tilde{U}_y^{\mathrm{P}}$, and $\tilde{U}_z^{\mathrm{P}}$ of the P-wavefield using equations 9 and 12. The inputs are the 3D Fourier transform of the original wavefield $\tilde{\mathbf{U}} = (\tilde{U}_x,\tilde{U}_y,\tilde{U}_z)$ and wavenumber $\mathbf{K}'$. The vector equation 9 contains three linear equations (one for each component) and equation 12 is one linear equation, so there are four equations and three unknown variables. Only two of the three equations in vector equation 9 are independent. Thus, any two of the equations in 9, along with equation 12, form a system of three independent linear equations, and the three unknown variables $(\tilde{U}_x^{\mathrm{P}},\tilde{U}_y^{\mathrm{P}},\tilde{U}_z^{\mathrm{P}})$ can be solved, for example, by Gaussian substitution. The solution for the three Fourier components of the P-wavefield is

$$\tilde{U}_x^{\mathrm{P}} = K_x^2\tilde{U}_x + K_xK_y\tilde{U}_y + K_xK_z\tilde{U}_z, \tag{15a}$$

$$\tilde{U}_y^{\mathrm{P}} = K_y^2\tilde{U}_y + K_yK_x\tilde{U}_x + K_yK_z\tilde{U}_z, \tag{15b}$$

and

$$\tilde{U}_z^{\mathrm{P}} = K_z^2\tilde{U}_z + K_zK_x\tilde{U}_x + K_zK_y\tilde{U}_y, \tag{15c}$$

where K_x, K_y, and K_z are K'_x, K'_y, and K'_z normalized by $|\mathbf{K}'|$ and thus are dimensionless, and $\mathbf{K} = (K_x,K_y,K_z)$. For example, $K_x = K'_x(K'^2_x + K'^2_y + K'^2_z)^{-1/2}$. The short form is

$$\tilde{\mathbf{U}}^{\mathrm{P}} = \mathbf{K}(\mathbf{K}\cdot\tilde{\mathbf{U}}). \tag{16}$$

Similarly, using equations 10 and 14, the S-wavefield decomposition can be solved in the wavenumber domain as

$$\tilde{U}^s_x = (K_y^2 + K_z^2)\tilde{U}_x - K_xK_y\tilde{U}_y - K_xK_z\tilde{U}_z, \tag{17a}$$

$$\tilde{U}^s_y = (K_x^2 + K_z^2)\tilde{U}_y - K_yK_x\tilde{U}_x - K_yK_z\tilde{U}_z, \tag{17b}$$

and

$$\tilde{U}^s_z = (K_x^2 + K_y^2)\tilde{U}_z - K_zK_x\tilde{U}_x - K_zK_y\tilde{U}_y. \tag{17c}$$

The short form is

$$\tilde{\mathbf{U}}^{\mathrm{S}} = -\mathbf{K}\times(\mathbf{K}\times\tilde{\mathbf{U}}). \tag{18}$$

In two dimensions, the expanded form of the decomposed P-wavefield in the (K_x,K_z) wavenumber domain is

$$\tilde{U}^{\mathrm{P}}_x = K_x^2\tilde{U}_x + K_xK_z\tilde{U}_z \tag{19a}$$

and

$$\tilde{U}^{\mathrm{P}}_z = K_z^2\tilde{U}_z + K_zK_x\tilde{U}_x. \tag{19b}$$

Similarly, the expanded form of the decomposed S-wavefield in the (K_x,K_z) wavenumber domain is

$$\tilde{U}^{\mathrm{S}}_x = K_z^2\tilde{U}_x - K_xK_z\tilde{U}_z \tag{20a}$$

and

$$\tilde{U}^{\mathrm{S}}_z = K_x^2\tilde{U}_z - K_zK_x\tilde{U}_x. \tag{20b}$$

Inverse Fourier transforms of $\tilde{U}^{\mathrm{P}}_x$, $\tilde{U}^{\mathrm{P}}_y$, and $\tilde{U}^{\mathrm{P}}_z$ in equation 15a–15c give the 3D vector components of the P-waves in (x,y,z). Inverse Fourier transforms of $\tilde{U}^{\mathrm{S}}_x$, $\tilde{U}^{\mathrm{S}}_y$, and $\tilde{U}^{\mathrm{S}}_z$ in equation 17a–17c give the 3D vector components of S-waves in (x,y,z). Inverse Fourier transforms of $\tilde{U}^{\mathrm{P}}_x$ and $\tilde{U}^{\mathrm{P}}_z$ in equation 19a and 19b give the 2D vector components of the P-waves in (x,z). Inverse Fourier transforms of $\tilde{U}^{\mathrm{S}}_x$ and $\tilde{U}^{\mathrm{S}}_z$ in equation 20a and 20b give the 2D vector components of the S-wave in (x,z).

Wavefield decomposition in anisotropic media

In isotropic media, the wavenumber $\mathbf{K}$ is not only the wave-propagation direction but also the P-wave-polarization direction. The P-wave and S-wave polarizations are perpendicular to each other, so polarization can be used as the basis of P- and S-wavefield decomposition. Using $\mathbf{A}^{\mathrm{P}}$ to represent the P-wave-polarization vector, equation 16 becomes

$$\tilde{\mathbf{U}}^{\mathrm{P}} = \mathbf{A}^{\mathrm{P}}(\mathbf{A}^{\mathrm{P}}\cdot\tilde{\mathbf{U}}) \tag{21}$$

and equation 18 becomes

$$\tilde{\mathbf{U}}^{\mathrm{S}} = -\mathbf{A}^{\mathrm{P}}\times(\mathbf{A}^{\mathrm{P}}\times\tilde{\mathbf{U}}), \tag{22}$$

where $|\mathbf{A}^{\mathrm{P}}| = 1$. Wavenumber $\mathbf{K}$ is valid only for wavefield decomposition in isotropic media, and polarization $\mathbf{A}^{\mathrm{P}}$ can be used in isotropic media and for anisotropic media of any symmetry (Dellinger, 1991). Dellinger (1991) was the first to present equation 21, but because his approach was different from that used here (he isolated the S-waves by subtracting the P-waves from the total wavefield), he did not find equation 22. In fact, neither Dellinger's wavefield subtraction nor equation 22 explicitly extracts the S-waves, but rather, they extract the non-P portion of the wavefield. More important, equations 21 and 22 form a pair that is an extension of the corresponding Helmholtz equations. Equations 21 and 22 are both necessary for completeness; equation 22 is the basis of our decomposition of S-waves into SV and SH in anisotropic media.

Like wavefield decomposition in isotropic media by equations 21 and 22, we also can decompose the anisotropic quasi-P and quasi-S waves (qP and qS) based on their polarizations (see Appendix A, which gives a physical interpretation of why wavefields can be decomposed). From this point on, we drop the redundant q in qP and qS whenever referring to anisotropic propagation; it should be understood to be present. In anisotropic media, the wavefield is also a linear superposition of P, SH, and SV. In the wavenumber domain,

$$\tilde{\mathbf{U}} = \tilde{\mathbf{U}}^{\mathrm{P}} + \tilde{\mathbf{U}}^{\mathrm{SH}} + \tilde{\mathbf{U}}^{\mathrm{SV}}, \tag{23}$$

where $\tilde{\mathbf{U}}^{\mathrm{P}} = (U^{\mathrm{P}}_x,U^{\mathrm{P}}_y,U^{\mathrm{P}}_z)$, $\tilde{\mathbf{U}}^{\mathrm{SV}} = (U^{\mathrm{SV}}_x,U^{\mathrm{SV}}_y,U^{\mathrm{SV}}_z)$, and $\tilde{\mathbf{U}}^{\mathrm{SH}} = (U^{\mathrm{SH}}_x,U^{\mathrm{SH}}_y,U^{\mathrm{SH}}_z)$. $\tilde{\mathbf{U}}^{\mathrm{P}}$, $\tilde{\mathbf{U}}^{\mathrm{SV}}$, and $\tilde{\mathbf{U}}^{\mathrm{SH}}$ are perpendicular to one another. The two conditions of linearity and perpendicularity allow the wavefield to be decomposed in VTI media.

What remains is to define the wave-polarization direction which, in an isotropic medium, is the unit wavenumber vector $\mathbf{K}$. In anisotropic media, wave-propagation direction is neither parallel nor perpendicular to the P-, SV-, or SH-wave polarizations, so $\mathbf{K}$ cannot be used directly. Fortunately, the Christoffel equation relates the wave-polarization direction and the wave-propagation direction $\mathbf{K}$ in anisotropic media.

The Christoffel equation is

$$[\mathbf{\Gamma} - \rho V^2\mathbf{I}]\mathbf{A} = 0. \tag{24}$$

In equation 24, $\mathbf{I}$ is the unit diagonal matrix; $\Gamma_{ik} = C_{ijkl}K_jK_l$, where C_{ijkl} is the elastic stiffness tensor; K_j and K_l are components of the normalized and dimensionless plane-wave-propagation direction $\mathbf{K}$ and $i,j,k,l = 1,2,3$ (consistent with Carcione, 2007); ρV^2 is an eigenvalue of matrix $\mathbf{\Gamma}$; and $\mathbf{A} = (A_x,A_y,A_z)^T$ is the corresponding eigenvector. Usually, there are three (unequal) eigenvalues of the 3×3 matrix, so they have three corresponding eigenvectors. Each $(A_x,A_y,A_z)^T$ is defined in the (K_x,K_y,K_z) wavenumber domain and is equal to $(K_x,K_y,K_z)^T$ for P-waves in isotropic media; ρ is density, and V is phase velocity. Equation 24 explicitly relates phase velocity to the wave-propagation direction.

In anisotropic media, there are three different eigenvalues of the Christoffel equation, so there are three perpendicular eigenvectors: $\mathbf{A}^{\mathrm{P}}(=A^{\mathrm{P}}_x,A^{\mathrm{P}}_y,A^{\mathrm{P}}_z)$ corresponds to the P-wave's eigenvector, $\mathbf{A}^{\mathrm{SV}}(=A^{\mathrm{SV}}_x,A^{\mathrm{SV}}_y,A^{\mathrm{SV}}_z)$ corresponds to the SV-wave's eigenvector, and $\mathbf{A}^{\mathrm{SH}}(=A^{\mathrm{SH}}_x,A^{\mathrm{SH}}_y,A^{\mathrm{SH}}_z)$ corresponds to the SH-wave's eigenvector. These are the polarization directions of the P-, SV-, and SH-waves, respectively. All three are unit vectors.

Therefore, the anisotropic equivalent of equation 21 is

$$\tilde{\mathbf{U}}^{\mathrm{P}} = \mathbf{A}^{\mathrm{P}}(\mathbf{A}^{\mathrm{P}}\cdot\tilde{\mathbf{U}}), \tag{25}$$

which decomposes the P-wave by replacing the P-wave's polarization (in the isotropic solution) with the P-wave's eigenvectors (for the anisotropic solution). Similarly,

$$\tilde{\mathbf{U}}^{SV} = \mathbf{A}^{SV}(\mathbf{A}^{SV}\cdot\tilde{\mathbf{U}}) \tag{26}$$

decomposes the SV-wave using the SV-wave's polarization, and

$$\tilde{\mathbf{U}}^{SH} = \mathbf{A}^{SH}(\mathbf{A}^{SH}\cdot\tilde{\mathbf{U}}) \tag{27}$$

decomposes the SH-wave using the SH-wave's polarization.

Alternatively, starting from equation 22, we have

$$\tilde{\mathbf{U}}^{S} = -\mathbf{A}^{P}\times(\mathbf{A}^{P}\times\tilde{\mathbf{U}}) \tag{28}$$

to decompose the S-wave, which includes both SH and SV. Then

$$\tilde{\mathbf{U}}^{SH} = -\mathbf{A}^{SV}\times(\mathbf{A}^{SV}\times\tilde{\mathbf{U}}^{S}) \tag{29}$$

decomposes SH from the S-wavefield, and

$$\tilde{\mathbf{U}}^{SV} = -\mathbf{A}^{SH}\times(\mathbf{A}^{SH}\times\tilde{\mathbf{U}}^{S}) \tag{30}$$

decomposes SV from the S-wavefield.

Three-dimensional inverse Fourier transforms of $\tilde{U}^{P}_{x}$, $\tilde{U}^{P}_{y}$, and $\tilde{U}^{P}_{z}$ in equation 25 give the 3D, 3-C decomposed P-wavefield in space. Three-dimensional inverse Fourier transforms of the decomposed components of equations 26–30 give the corresponding 3D, 3-C decomposed $\mathbf{U}^{P}$, $\mathbf{U}^{S}$, $\mathbf{U}^{SV}$, and $\mathbf{U}^{SH}$ wavefields in space.

The main steps involved in wavenumber-domain decomposition are similar to those for a wavenumber-domain filter. The data are Fourier-transformed from the space domain to the wavenumber domain, the transform is multiplied by the chosen decomposition operator, and then an inverse transform takes the decomposed data back to the space domain. The fact that the waves are propagating is not relevant to the decomposition because only the wavefield values and their (spatial) derivatives are used. The decomposition is of a fixed-time snapshot, so the time dimension plays no role. The wavefields before and after decomposition are at exactly the same spatial locations; there are no phase shifts or propagation factors between the input and output wavefields.

This method can be extended for inhomogeneous anisotropic wavefield decomposition. The anisotropic phase polarization is local, not global (Nistala and McMechan, 2005), so the wavefield decomposition needs to be done separately for each region that has a different polarization distribution. Then the decomposed wavefields in each region need to be joined into the composite wavefields for each wave type (P, SH, and SV) across the whole model.

Because wavefield displacements (and particle velocities) are continuous, the boundary conditions are implicitly satisfied from region to region when decomposing P- and S-waves. At discontinuities in the elastic tensor values, the boundary is assumed to be infinitely thin, so each grid point is either in one polarization distribution or the other for the Christoffel equation 24. At a reflection point, a wavefront will have a change of sign of wavenumber so the incident and reflected contributions will correspond to different parts of the same decomposition operator.

Decomposition is based on polarization. Different parts of a wavefront may have different polarizations, but each will be treated individually by its respective decomposition operator. If different regions of a model have the same polarization distribution, one decomposition (and one inverse Fourier transform) is sufficient (Appendix B). This is the reason that the decomposition for an isotropic medium is global and does not depend on local velocity distribution. If polarization can be determined independently (for example, by direct measurements from 3-C data) (Gomes et al., 2004; Agnihotri and McMechan, 2007), then estimation of polarization via the Christoffel equation is not required.

Decomposition becomes expensive if the medium has many regions with different polarization distributions because the inverse transform needs to be done once for each decomposition operator in each polarization distribution. However, it may be possible to get approximate decompositions by treating groups of points with similar polarization distributions as if they are the same (see Dellinger, 1991) for an example of an approximate separation for an orthorhombic medium using a VTI separation operator).

EXAMPLES

This section contains three elastic examples. They are for a 2D heterogeneous isotropic model, a 2D heterogeneous anisotropic model, and a 3D heterogeneous anisotropic model.

The layer geometry in the 2D examples is shown in Figure 3 and the elastic tensor elements are given in Table 1. For the isotropic example, the P-wave velocities increase from 1500 to 4000 m/s from layer 1 to layer 6, and the S-wave velocities increase from 500 to 2000 m/s. For the anisotropic example, layer 1 is isotropic and the other six layers are transversely isotropic with a vertical symmetry axis (VTI). The velocity anisotropy is about 10% for the P- and S-waves. The horizontal P and S velocities are the same as the P- and S-wave velocities, respectively, in the isotropic model. An explosive source at the top of layer 1 (Figure 3) has a Ricker-wavelet time dependence for both isotropic and anisotropic models.

Two-component, 2D fixed-time snapshots are generated for the isotropic and anisotropic versions of the model in Figure 3 using finite differences on a staggered grid with eighth-order differential operators in space and second-order operators in time. The perfectly matched layer-absorbing boundary condition (Komatitsch and Martin, 2007) is applied to all four grid edges. The same algorithm is applied to generate the 3-C, 3D example below.

2D isotropic elastic wavefield decomposition

Figure 4a and d shows the x- and z-components of the input 2D (particle-velocity) wavefields at time = 0.7 s. Figure 4b, c, e, and f contains the decomposed wavefields obtained by using the proposed method. The amplitude and phase of the decomposed x- and

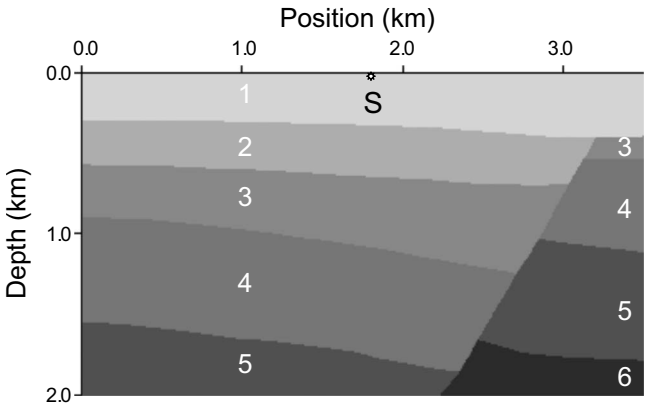

Figure 3. This is the velocity geometry for both the 2D isotropic and anisotropic models. The numbers 1, 2, 3…, 6 identify the layer properties in Table 1. S is the source location.

Table 1. Tensor element values (in Pa) for each layer in the 2D isotropic, 2D VTI, and 3D VTI models. For the isotropic 2D model, only C11 and C55 are used. For the 2D VTI model, only C11, C33, C13, and C55 are used. For the 3D model, only layers 1 through 4 are used. The vertical (3) axis is the symmetry axis.

	Elastic tensor elements					
	Layer 1	Layer 2	Layer 3	Layer 4	Layer 5	Layer 6
C_{11}	5.0E + 09	7.0E + 09	9.0E + 09	1.0E + 10	1.2E + 10	1.4E + 10
C_{13}	1.0E + 09	1.3E + 09	2.1E + 09	2.2E + 09	1.9E + 09	2.1E + 09
C_{33}	5.0E + 09	8.0E + 09	9.9E + 09	1.2E + 10	1.4E + 10	1.7E + 10
C_{55}	2.0E + 09	3.8E + 09	3.9E + 09	4.9E + 09	5.9E + 09	6.7E + 09
C_{12}	1.0E + 09	1.2E + 09	2.0E + 09	2.0E + 09	N/A	N/A

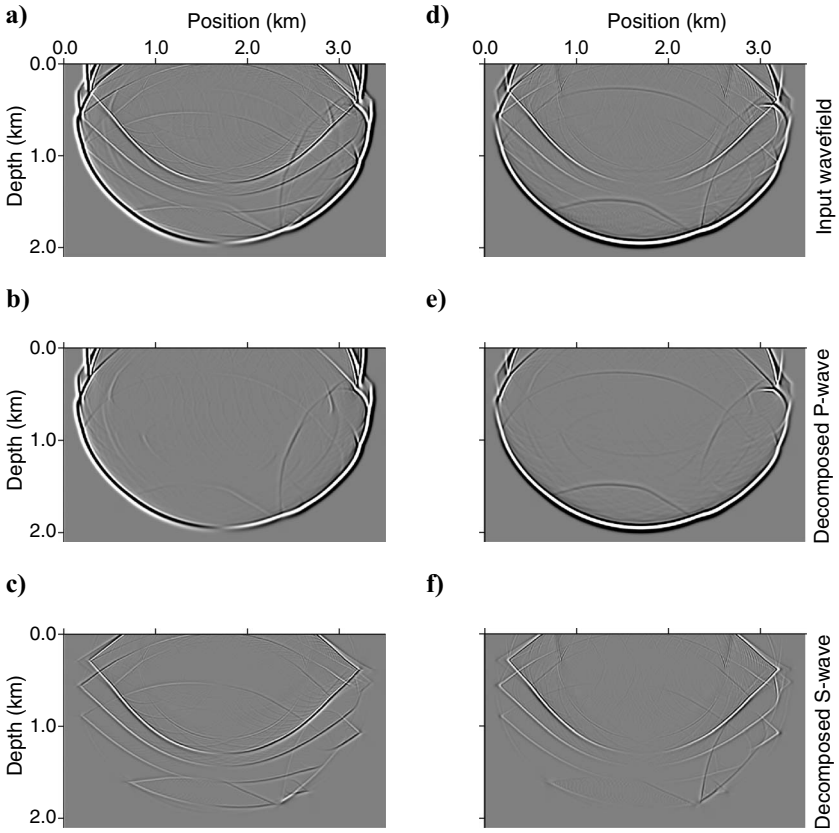

Figure 4. Wavefield decomposition in the isotropic 2D model of Figure 3 using the proposed method. (a,d) are the x- and z-components of the input wavefield. (b,e) are the x- and z-components of the decomposed P-wave. (c,f) are the x- and z-components of the decomposed S-wave. Decomposition is good; the components are well separated, and phase, amplitude, and physical units are correct.

z-components of the P- and S-waves are equal to those of input P- and S-wavefields. The decomposed P- and S-wavefields do not include each other. For comparison, Figure 5 shows the divergence and curl results (Sun and McMechan, 2001). Because of the derivatives in the divergence and curl operations, the waveform and phase are changed, and more important, the physical unit is changed. For example, if the input wavefield is particle displacement, the spatial derivatives are dimensionless (meters/meters), and if the input wavefield is particle velocity, the spatial derivatives have units of seconds^{-1} (meters/[seconds·meters]). In Figure 5, the waves have been separated by divergence and curl operations and thus have a 90° phase shift (see the "Discussion" section below).

Alternatively, the x- and z-components of the P-wave can be obtained by subtracting the decomposed x- and z-components of the S-wave from the original input x- and z-component wavefields. Similarly, the x- and z-components of the S-wave can be obtained by subtracting the decomposed x- and z-components of the P-wave from the x- and z-components of the original input wavefield. The difference between the subtracted S-wave (or P-wave) and the decomposed S-wave (or P-wave) components is negligible.

2D anisotropic elastic wavefield decomposition

Wavefield decomposition in the wavenumber domain depends on the orthogonality of the different wave types. The wavefield-polarization distribution in an isotropic medium is global; however, the polarization direction in anisotropic media is local. Thus, wavefields that have different polarization distributions need to be decomposed separately using their different Christoffel eigenvectors.

For this example, the six-layer geometry is the same as the previous isotropic example (Figure 3). Table 1 contains the values of the elastic tensor elements. Because the anisotropic polarization is local, the wavefield is divided into six isolated zones, one within each layer. The wavefield present within each layer is decomposed using its local anisotropic polarization distributions and decomposition operators. Therefore, six local wavefield decompositions are performed for this example. The full decomposition involves 24 2D inverse Fourier transforms (six layers × two operators [one for P-waves and one for S-waves] × two components [x and z]). The number of inverse transforms is reduced to 12 if only P-waves are decomposed and then wavefield subtraction is used to produce the S-waves (or vice versa). Then the P portions of the six decomposed wavefields are combined to construct a complete decomposed P-wavefield. Similar, all the S portions are combined into

the single composite S-wavefield. This method is also applied to the 3D wavefield decomposition in inhomogeneous anisotropic media in the next section.

Figure 6 contains the same information as Figure 4 but for the wavefields in the 2D VTI model at time = 0.7 s. The decomposition is successful because the amplitude and phase of the decomposed P- and S-wave components are equal to those of P- and S-waves in the input wavefield. For comparison, Figure 7a and c shows the divergence and curl results, in which the separation is not complete. The P-wave part (Figure 7a) has S-wave artifacts, and the S-wave part (Figure 7b) has P-wave artifacts. Figure 7b and d shows the divergencelike and curllike results, using Dellinger and Etgen's (1990) algorithm. These results are better than those shown in Figure 7a and b because the P- and S-waves are separated, but they have a residual $\pi/2$ phase shift.

The proposed method (Figure 6) not only separates the P- and S-waves (the polarization is correct, and P and S do not include each other) but also has correct phase, amplitude, and physical units (see the "Discussion" section below). In two dimensions, SV is the only S-wave present. Similar to the wavefield decomposition in isotropic media, the x- and z-components of the P-wave can be obtained by subtracting the x- and z-components of the S-wave from the original input x- and z-component wavefields, and vice versa. Dellinger (1991) uses this as a key part of his approach to obtain the S-waves.

3D anisotropic elastic wavefield decomposition

The wavefield decomposition also works in 3D, heterogeneous, VTI anisotropic structure. As for the wavefield decomposition in 2D, heterogeneous, anisotropic structure, the wavefield decomposition in three dimensions needs to be done separately for each region that has a different polarization distribution. Then the pieces are compiled into the composite P-, SV-, and SH-wavefields for the whole model.

Consider the 3D geometry in Figure 8. The symmetry in all four layers is VTI. The anisotropies of the P- and S-wave velocities are about 10%. Table 1 contains the elastic tensor values. The finite-difference algorithm used to generate the synthetic test data is a 3D version of that used for the 2D model in the previous section. A force source with orientation (1,1,1) that has a Ricker time dependence is located in the center of the model (Figure 8).

Figure 9 shows snapshots of the 3-C input wavefield and the decomposed x-, y-, and z-components of P, SV, and SH (using equations 25–27) on a vertical y-z slice through the source, all at time = 0.35 s. The decomposed x-components of P, SH, and SV do not include one another, and their sum equals the x-component of the input wavefield; the same is true for the y- and z-components. As expected, the z-component of SH is zero everywhere (because the SH-wave-polarization direction is perpendicular to the z-axis), and the x-(transverse) component of the direct P-wave is close to zero (the theoretical value for this model) in the layer in which the source is located.

The snapshots in Figure 10 are located on a vertical x-z slice, which is perpendicular to that in Figure 9, and goes through the source at the same time. The layout of Figure 10 is the same as that of Figure 9. As in Figure 9, the x-components of the decomposed P-, SH-, and SV-waves do not include one another, and their sum is equal to the input x-component wavefield; the same is true for the y-

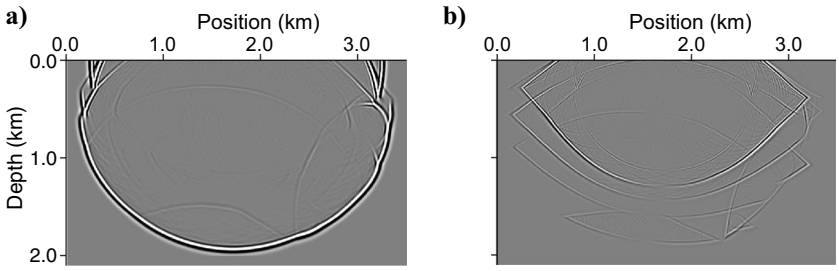

Figure 5. (a,b) are the divergence and curl of the wavefield of Figure 4a and d. Phase, amplitude, and physical units are not correct (Sun and McMechan, 2004).

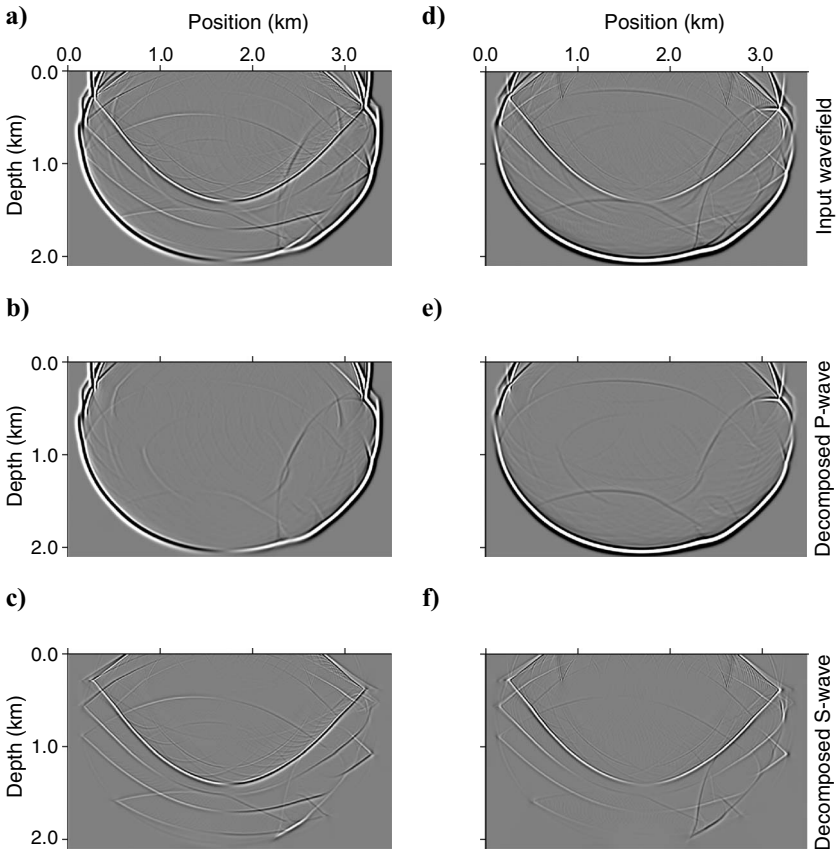

Figure 6. Wavefield decomposition in the anisotropic 2D model using the proposed method. (a,d) are the x- and z-components of the input wavefield. (b,e) are the x- and z-components of the decomposed P-wave. (c,f) are the x- and z-components of the decomposed S-wave. Decomposition is good; the P- and S-waves are well separated, and their phase, amplitude, and physical units are correct.

and z-components. Again, the z-component of SH is zero everywhere, and the y-component of P is close to zero (the theoretical value for this slice). The decomposed P-, SH-, and SV-waves are well separated; none includes the others, and they have the correct amplitude, phase, and physical units. The alternative sequence of equations 21 and 28–30 was also performed, and it produced identical results. Thus, the 3-C, 3D anisotropic wavefield decomposition is successful.

The examples above show the ability to handle crossovers by enforcing continuity of polarization. For 3D VTI media, there is a kiss singularity in S1 and S2 at $K_z = \pm 1$ (Figure 2) as a result of the coincidence of the longitudinal and transverse polarizations. These singularities continue to exist in the x- and y-components of SV and SH (Figures 9 and 10). If these points are avoided (e.g., Dellinger, 1991), then the present approach is still viable. In the z-components of SV in Figures 9 and 10, there is no kiss singularity because the SH component is zero in this direction. Finding the solution of the singularity problem is a challenge for future work; it is not solvable at this time.

The polarization directions of the SH- and SV-waves cannot be identified from the S-wave at a kiss singularity point. Even though the number of grid points in the kiss singularities is a small part of the whole wavefield for the example in Figures 8–10, each singular point affects many more points in the wavefields because the inverse Fourier transform is global (Figures 9 and 10).

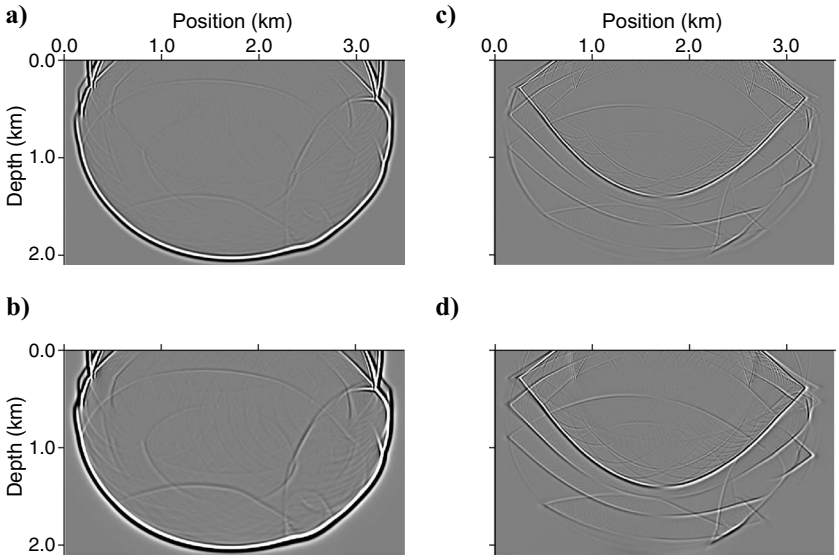

Figure 7. Panels (a,c) are divergence and curl of the input wavefield (Figure 6a and d); (b,d) are the corresponding divergencelike and curllike separations. The (a) divergence method and (c) curl method cannot separate the wavefield in anisotropic media; the P-wave includes some S-wave energy, and vice versa. The (b) divergencelike and (d) curllike operators can separate P- and S-waves, but their phase, waveform, and physical units are not correct.

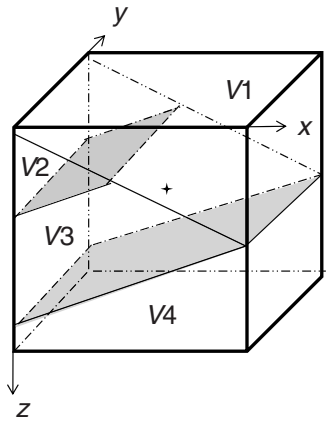

Figure 8. The 3D VTI model used to illustrate wavefield decomposition in arbitrarily heterogeneous structure. The dimensions of the computational grid are 250 × 250 × 250 points (1500 m × 1500 m × 1500 m). The horizontal P-wave velocities ($V1$ to $V4$) vary from 1500 m/s to 3000 m/s, and the S-wave velocities vary from 1000 m/s to 1500 m/s.

DISCUSSION

Several related topics have not been discussed above because they are not central to the current goals, but they can add to the overall understanding of the larger subjects of wave separations and singularities. Two of these topics, which have been described by Dellinger (1991), are (1) that there are no singularities in two dimensions because there is only one P-wave and one (in-plane) S-wave, which have nonoverlapping slownesses, and (2) shear-wave singularities are necessary in three dimensions because it is not geometrically possible to have globally continuous particle motions. Dellinger (1991) also shows his separation operators in the space domain and shows an approximate orthorhombic separation operator. The following subsections contain a series of other observations that define still unanswered questions that are salient topics for future research.

Relation to and differences from previous methods

Appendix C contains a summary of the key relations among the various previous, current, and possible future approaches. Here we highlight only previous methods. P- and S-wave separation, using divergence

$$\underline{U}^{\mathrm{P}} = \nabla \cdot \mathbf{U} \tag{31}$$

and curl

$$\underline{\mathbf{U}}^{\mathrm{S}} = \nabla \times \mathbf{U} \tag{32}$$

in isotropic media has been done by Sun and McMechan (2001). The underlines indicate the wavefields separated by this (traditional) method (see Appendix C). This is a special case of wavefield separation (in fact, a wavefield transformation, not a decomposition) in which propagation direction is parallel or perpendicular to polarization direction. In general, in anisotropic media, wave-propagation direction is not parallel or perpendicular to wave-polarization direction. If the original wavefield is a particle-velocity vector wavefield $\mathbf{U}$, $\underline{U}^{\mathrm{P}}$ is a scalar with units of s^{-1}, and $\underline{\mathbf{U}}^{\mathrm{S}}$ is a vector, also with units of s^{-1}. More important, there is a 90° phase shift in the output relative to the input (Sun et al., 2001).

Dellinger and Etgen (1990) take advantage the perpendicular relationship of P and SV in VTI media to separate P- and SV-waves in the wavenumber domain and then do inverse Fourier transforms to

obtain the separated P- and S-wavefields in the space domain. Their method (for anisotropic media) is

$$\tilde{\underline{U}}^{\mathrm{P}} = i\mathbf{A}^{\mathrm{P}} \cdot \tilde{\mathbf{U}} \tag{33}$$

and

$$\tilde{\mathbf{U}}^{\mathrm{S}} = i\mathbf{A}^{\mathrm{P}} \times \tilde{\mathbf{U}}. \tag{34}$$

This method, based on divergence and curl, extends their concept into anisotropic wavefield separation. We call these divergencelike and curllike wavefield separations. Similar to the isotropic, the waves separated by divergencelike and curllike operator equations 33 and 34 have lost their original physical meaning, and the units are changed by the spatial derivative. The multiplication by i in equations 33 and 34 corresponds to a 90° phase shift.

The amplitudes of the separated wavefield in the wavenumber domain, obtained by the divergence and curl methods, keep the correct amplitude (equations 31 and 32 and equations 33 and 34). However, the 90° phase shift changes the energy distribution in the space domain; the waveforms after separation are different from those of the original wavefield. Dellinger and Etgen (1990) discuss the consequences of the 90° phase shift.

An alternative separation operator is presented by Yan and Sava (2009), who use local pseudoderivative operators in the space domain. The space-domain equivalents of the separation operators are more compact when they have a derivative in them. Thus, an analogy can be drawn between the space- and wavenumber-domain separations and the space- and wavenumber-domain derivative calculations. Yan and Sava's (2009) algorithm is analogous to finite-difference calculations, and Dellinger and Etgen's (1990) algorithm is analogous to pseudospectral calculations. The former can handle locally smooth changes in polarization but is a less accurate approximation, whereas the latter is more accurate but is less efficient when polarization changes rapidly in space. The latter also applies to our wavenumber-domain decomposition. There is no known decomposition that operates in the space domain (other than the Helmholtz integral solution, which is very inefficient; Appendix C).

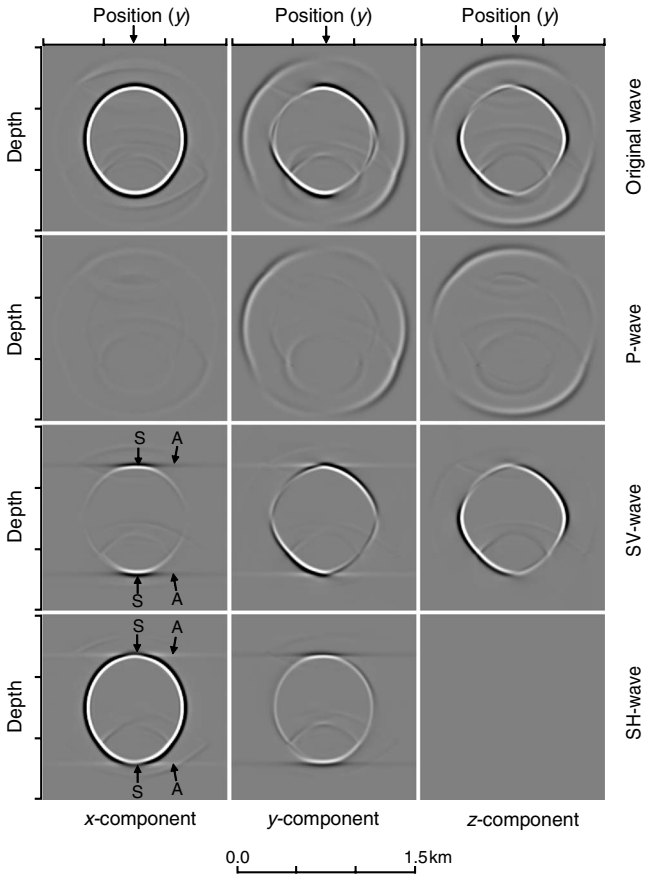

Figure 9. Snapshots on the y-z profile through the source at time = 0.35 s; the arrows in the upper three panels point to the y-coordinate of the source and the location of the x-z profile in Figure 10. All of the panels have the same coordinates and amplitude scaling. The vertical columns from left to right are the x-, y-, and z-components. The rows from top to bottom are the input wavefield and the decomposed P-, SV-, and SH-wavefields. No decomposed wave component includes the others. In the SV and SH panels, artifacts A are associated with singularities S.

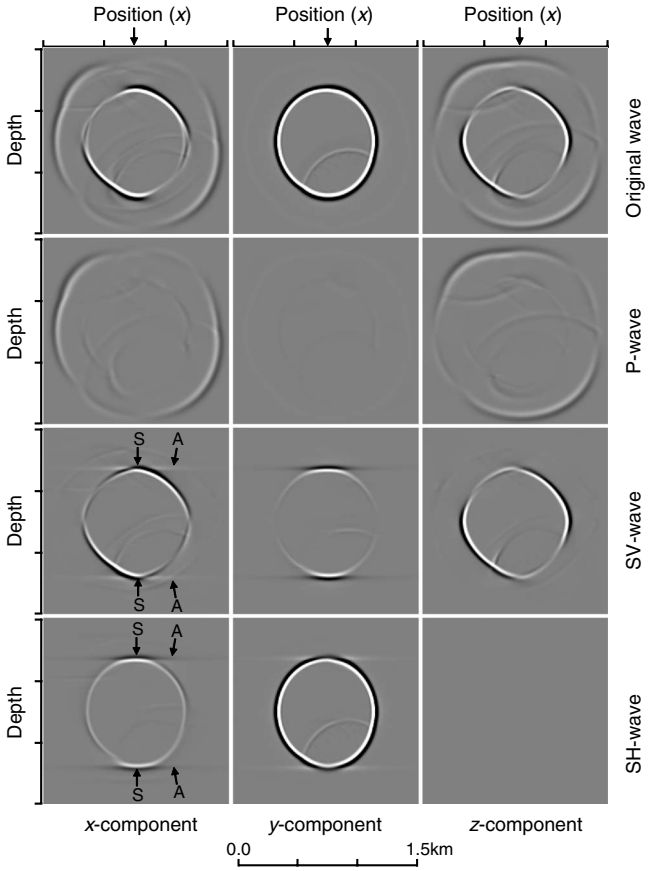

Figure 10. Snapshots on the x-z profile through the source at time = 0.35 s; the arrows in the upper three panels point to the x-coordinate of the source and the location of the y-z profile in Figure 9. All of the panels have the same coordinates and amplitude scaling. The vertical columns from left to right are the x-, y-, and z-components. The rows from top to bottom are the input wavefield and the decomposed P-, SV-, and SH-wavefields. No decomposed wave component includes the others. In the SV and SH panels, artifacts A are associated with singularities S.

Decomposition of SV and SH in 3D anisotropic media

In a 2D VTI medium, there are only two types of waves (P and SV) (Figure 6). Thus, there are no singularities because only one S-wave exists, and the S-polarization is unique. In a 3D anisotropic medium, the S-wave splits into SV and SH (Figures 9 and 10). In any vertical 2D slice containing the symmetry axis through the 3D polarization distribution, both kiss and crossover singularities are present (Figure 1). In other 2D slices, the kiss singularity will not be present, and crossovers may or may not be present (visualize planes cut through the origin of the 3D polarization distribution in Figure 1). Dellinger and Etgen (1990) avoid singularities by considering only 2D VTI media. Dellinger (1991) shows only the z-component of the 3D response (in which there is no SH-wave [Figures 9 and 10] and thus no singularity). Yan and Sava (2009) also consider only 2D VTI examples and therefore also avoid singularities.

Here we use the wave polarization (Figure 2) rather than fast or slow (S1 or S2) S-waves (Figure 1) to define SV and SH. The polarization gives continuous SH and SV polarization surfaces (Figure 2) except at the kiss singularities at $K_z = \pm 1$ (Dieulesaint, 1974; Červený, 2001; Carcione, 2007; Tsvankin, 2005). One of the polarization surfaces (SV or SH) can be faster or slower than the other, depending on the propagation direction. SV and SH are more physically meaningful than S1 and S2. The pairs of equations 26 and 27 and 29 and 30 use this concept to do the S-wave decomposition.

The examples above are for VTI media only. The P-wave decompositions are easy to obtain because the velocity of the P-waves is always faster than that of the S-waves (so it is easy to extract the P-wave-polarization distribution) for any kind of anisotropy (Dellinger, 1991). The S-waves can be obtained by subtracting the P-waves from the total wavefield (Dellinger, 1991) or, for VTI, by using equation 22. Further decomposition of the S-waves can be done by equations 29 and 30 for VTI and triclinic media if singularities are avoided (V. Grechka, personal communication, 2009). However, for media with lower symmetries, the slowness surfaces become more complicated, and it is more difficult to systematically identify and extract S-wave polarizations (Dellinger, 1991). Decompositions of such wavefields have not yet been done and may not be possible. In any case, that is beyond the scope of this paper.

Staggered grid

In a regular nonstaggered grid, all of the elastic tensor element and field variables are defined at the same grid locations. In a staggered-grid design, the variables that are used to do the decomposition are not all located at the same points, so we cannot do the wavefield decomposition directly. We need to do some interpolation to estimate the needed values at common grid points. For example, if variable u is defined as $u[(n+1/2)\Delta x]$ (there is no definition of u at $(n\Delta x)$), we use the average $0.5*\{u[(n+n+1/2)\Delta x] + u[(n-[(n+1/2)\Delta x])\Delta x]\}$ to estimate $u(n\Delta x)$. Dellinger and Etgen (1989) also use the analog of staggered differencing in their separation operators.

Summary

The key results of this paper are equations 16 and 18 for decomposing isotropic wavefields, and equations 21 and 22 for decomposing anisotropic wavefields. The approach in both cases is the same; we have shown derivations, examples, and how to understand and interpret the procedure. In doing this, we have verified the ideas presented by Dellinger and Etgen (1989, 1990) by independently deriving similar relations in a more rigorous way and extending them into a more complete theoretical framework (see Appendix C). The latter provides the formalism for decomposing SV and SH from S (except for the kiss singularities), which had not been done previously.

Finally, it is important to reiterate the practical motivation for developing this topic. For a prestack elastic migration to produce accurate images of P, S, and converted P-S and S-P reflection coefficients, it is necessary to have all the P- and S-waves decomposed in both the source and receiver wavefields at the image locations before applying the image condition. For example, elastic extrapolation of a recorded common-source wavefield containing P and P-S converted reflections will result in spatial and temporal coincidence of these reflections at the image time. The resulting migrated image amplitudes are an interfering mixture of the P and P-S reflection coefficients unless they are explicitly decomposed. The vector decomposition is also a prerequisite to full-wavefield inversion for elastic tensor elements, as described by Tarantola (1988) and by Caricone (2007). Because the wavefield components and hence propagation directions are available after wavefield decomposition, common-angle gathers are directly available for AVA analysis. The wavefield-propagation direction can also be obtained by applying Yan and Sava's (2009) pseudoderivative operators to equations 21, 22, 29, and 30 (Ma and Zhu, 2003; Jianlei et al., 2007).

Surface and interface waves will also have their corresponding polarizations and thus can be decomposed if they can be defined in terms of polarization. For example, Love-wave polarization is the same as SH and thus is expected to be decomposed along with SH-waves. Propagation of inhomogeneous waves involves complex wavenumbers.

CONCLUSIONS

A new vector decomposition based on polarization is derived. Two sequential vector (dot or cross-product) operations produce the decompositions of the P- and S-wavefields, respectively, as implied by Helmholtz's theory. The decomposed P- and S-wavefields have the same amplitude, phase, and physical units as the input wavefields, regardless of what the original wavefield was (displacement, velocity, or acceleration). This method is extended for decomposing a wavefield in inhomogeneous VTI media into vector components of P-, SH-, and SV-waves. The key to decompose SV and SH waves is to define SV and SH surfaces based on polarization rather than defining S1 and S2 (fast and slow) velocities based on the eigenvalues of the Christoffel equation. Because the polarizations are local rather than global, decompositions are done separately for each region that has a different polarization distribution. The P-, SV-, and SH-waves in each region are combined into the composite P-, SV-, and SH-wavefields that span the model. Decomposition works well in VTI media except at the singular points at $K_z = \pm 1$.

Future potential applications include two key aspects of reverse time migration. The first is decomposition of overlapped P and P-to-S converted reflections at the image time (because they satisfy the same image condition). The second is that incident and reflected angles can be easily calculated from the decomposed vector components of the source and receiver wavefields as part of the image condition. Other possible applications include estimation of the orientation of symmetry axes and amounts of shear-wave splitting.

ACKNOWLEDGMENTS

The research leading to this paper was supported by the Sponsors of the University of Texas at Dallas Geophysical Consortium and by the Petroleum Research Fund of the American Chemical Society under grant 47347-ACS. We thank Joe Dellinger for helpful discussions at the start of this project. Constructive comments by Vladimir Grechka, Mirko van der Baan, Joe Dellinger, and three anonymous reviewers are much appreciated. This paper is Contribution No. 1207 from the Department of Geosciences at the University of Texas at Dallas.

APPENDIX A

USING WAVEFIELD POLARIZATION FOR WAVEFIELD DECOMPOSITION: A PHYSICAL INTERPRETATION

In an anisotropic medium, the original wavefield $\tilde{\mathbf{U}}$ is a linear superposition of the polarized P-, SH-, and SV-waves (equation 21), whose polarizations are perpendicular to each other. The Christoffel equation defines the relationships between the wave-propagation direction and the polarization directions of the P-, SH-, and SV-waves. These allow an anisotropic wavefield to be decomposed; the vector decompositions are illustrated in Figures A-1 and A-2.

The domain in Figures A-1 and A-2 is wavenumber (K_x,K_y,K_z). At a location $\mathbf{K}$, which defines the wave-propagation direction, there is an input wavefield-polarization vector $\tilde{\mathbf{U}}$ with components $\tilde{\mathbf{U}}^{\mathrm{P}}$, $\tilde{\mathbf{U}}^{\mathrm{SV}}$, and $\tilde{\mathbf{U}}^{\mathrm{SH}}$. The eigenvectors of the Christoffel equation give the directions of $\tilde{\mathbf{U}}^{\mathrm{P}}$, $\tilde{\mathbf{U}}^{\mathrm{SV}}$, and $\tilde{\mathbf{U}}^{\mathrm{SH}}$. In isotropic media, the P-wave's polarization and $\mathbf{K}$ are in the same direction, but in anisotropic media, they are not.

Figure A-1, corresponding to equation 21, gives the physical procedure for the two-step decomposition of the P-wave. In the first step, the input wavefield polarization $\tilde{\mathbf{U}}$ projects onto the P-wave's polarization $\mathbf{A}^{\mathrm{P}}$ and gives the P-wave's scalar amplitude $|\tilde{\mathbf{U}}^{\mathrm{P}}| = |\tilde{U}^{\mathrm{P}}|$. The second step is to redistribute this scalar (by multiplying it by the vector components of the P-wave-polarization direction $\mathbf{A}^{\mathrm{P}}$) to recover the vector which has the correct phase and amplitude and, more important, the same physical units as input wavefields.

Similarly, Figure A-2, corresponding to equation 22, shows the S-wave decomposition by the two-cross-product method. The polarization direction of the S-wave is perpendicular to that of the P-wave. The first cross product $\mathbf{A}^{\mathrm{P}} \times \tilde{\mathbf{U}}$ in the wavenumber domain (which is Dellinger and Etgen's [1990] method, except for the phase shift) gives the remaining (S) wavefield ($\mathbf{N}$). The second product $-\mathbf{A}^{\mathrm{P}} \times \mathbf{N}$ recovers the correct amplitude, phase, and direction of $\tilde{\mathbf{U}}^{\mathrm{S}}$ in the wavenumber domain.

APPENDIX B

WAVEFIELD DECOMPOSITION OPERATORS DO NOT CHANGE IF $C_{ijk\ell}$ IS MULTIPLIED BY A SCALAR

Consider a P-wave with polarization distribution $\mathbf{A}^{\mathrm{P}}(K_x,K_y,K_z)$ in the wavenumber domain, where K_x, K_y, and K_z are the coordinates of a point in the normalized 3D wavenumber domain. If the polarizations of different elastic tensors have the same distribution in the wavenumber domain, they will have the same decomposition operators in the wavenumber domain (equations 21 and 22).

Thus, if a model is composed of different elastic tensors at different spatial locations but all of them have the same polarization distribution, they can be decomposed with the same decomposition operators and be restored into the space domain with a single inverse 3D Fourier transform for each decomposition operator. This has a major impact on the cost of the decomposition compared to doing an inverse Fourier transform for points that have different velocities, so we need to define under what conditions this is true.

Consider the relation between an eigenvalue λ and its eigenvector A, for matrix $\mathbf{\Gamma^0}$:

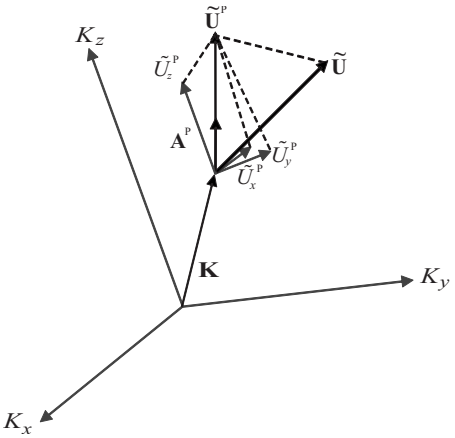

Figure A-1. The procedure for decomposing the P-wave. In the first step, $\tilde{\mathbf{U}}$ projects onto the P-wave's polarization $\mathbf{A}^{\mathrm{P}}$ to give the P-wave's amplitude $|\mathbf{U}^{\mathrm{P}}|$, which is a scalar (and is the same as Dellinger and Etgen's [1990] procedure, except for the phase shift). The second step is to redistribute to the scalar by multiplying $|\mathbf{U}^{\mathrm{P}}|$ by the components of $\mathbf{A}^{\mathrm{P}}$, to recover the vector, which has the correct phase and amplitude and, more important, the same physical meaning as the input wavefield.

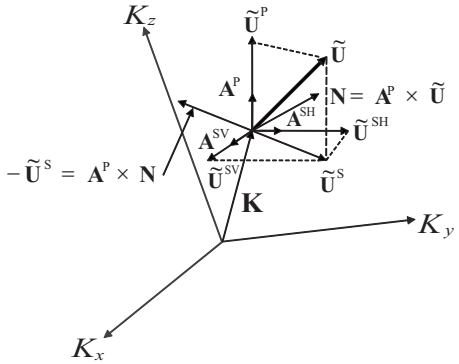

Figure A-2. The procedure for $\tilde{\mathbf{U}}^{\mathrm{S}}$ decomposition. The S-wave's polarization direction $\tilde{\mathbf{U}}^{\mathrm{S}}$ is perpendicular to that of the P-wave $\tilde{\mathbf{U}}^{\mathrm{P}}$. Therefore, the cross product of $\tilde{\mathbf{U}}$ with $\tilde{\mathbf{U}}^{\mathrm{P}}$ extracts the S-wave's curl-like vector ($\mathbf{N}$); this is Dellinger and Etgen's (1990) method except for the phase shift. The cross-product vector $\mathbf{N}$ is perpendicular to the correct S-wave polarization. The second step is to recover the decomposed vector $\tilde{\mathbf{U}}^{\mathrm{S}}$ by $-\mathbf{A}^{\mathrm{P}} \times \mathbf{N}$.

$$\mathbf{\Gamma^0} A = \lambda A, \tag{B-1}$$

where $\Gamma^0_{ik} = C^0_{ijk\ell} K_j K_\ell$. Let an inhomogeneous elastic tensor $C_{ijk\ell}(x,y,z) = g(x,y,z) C^0_{ijk\ell}$, where $g(x,y,z) \neq 0$ is any constant coefficient at the grid point (x,y,z). Then the elements Γ_{ik} in the Christoffel equation 24 change with position (x,y,z) as

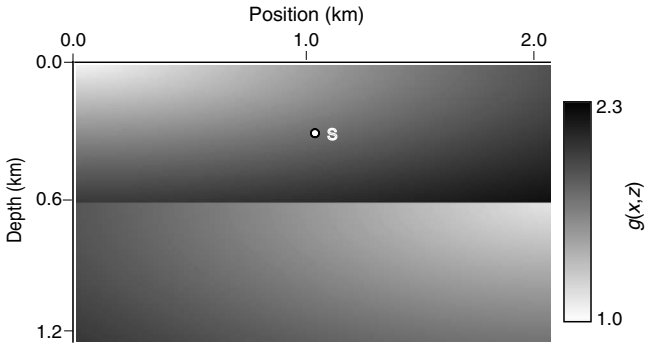

Figure B-1. This is a representative $g(x,z)$ distribution (equation B-2) used to illustrate the 2D result. The distribution $g(x,z)$ scales the elastic tensor $C^0_{ijk\ell}$ and hence the relative velocities from point to point. Thus, the boundary at 0.6-km depth is a velocity discontinuity which produces reflections (Figure B-2). However, the VTI polarization distribution does not change, and thus the decomposition operators are the same at all grid points.

$$\Gamma_{ik} = g(x,y,z) C^0_{ijk\ell} K_j K_\ell, \tag{B-2}$$

and equation B-1 becomes

$$\mathbf{\Gamma} A = g\lambda A. \tag{B-3}$$

Thus, $\mathbf{\Gamma}$ in equation B-3 and $\mathbf{\Gamma^0}$ in equation B-1 have the same eigenvector A for a given (K_i, K_j) pair because they have the same coordinates in the normalized wavenumber domain. The eigenvalue λ for $\mathbf{\Gamma^0}$ becomes $g\lambda$ for $\mathbf{\Gamma}$. From equations B-2 and 24, it is concluded that any medium that satisfies $C_{ijk\ell}(x,y,z) = g(x,y,z) C^0_{ijk\ell}$ will have a single unique polarization distribution, regardless of the variation in $g(x,y,z)$. Because $C^0_{ijk\ell}$ is the same for all (x,y,z), this defines a medium in which the symmetry of the anisotropy is the same from point to point but values of all the velocities may change subject to keeping the relative values prescribed by $C^0_{ijk\ell}$. A VTI medium with spatially variable velocities satisfies this requirement, as do isotopic and triclinic media.

Figure B-1 shows the $g(x,z)$ distribution for a 2D, heterogeneous, elastic anisotropic model with a single $C^0_{ijk\ell}$ but variable g. The corresponding x- and z-components of the wavefield produced by the source S in Figure B-1 are shown in Figure B-2a and B-2d. The resulting decomposed P- and S-waves are in Figure B-2b and B-2e and Figure B-2e and B-2c, and B-2f, respectively. These decompositions were produced with one inverse 2D Fourier transform for the P-waves and a second one for the S-waves because all points in the model have the same polarization and the same eigenvector.

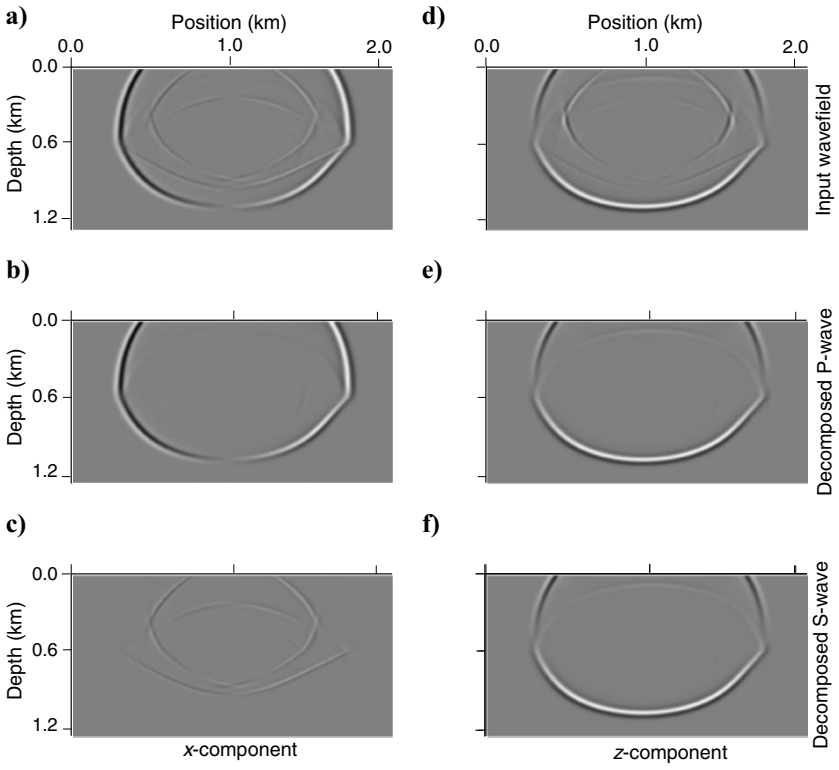

Figure B-2. (a,d) Input and decomposed (b,e) P and (c,f) S snapshots at time 0.3 s for the elastic VTI model composed of the single elastic VTI tensor for layer 2 in Table 1 and the $g(x,z)$ distribution in Figure B-1.

APPENDIX C

RELATIONS AMONG DIFFERENT APPROACHES TO WAVEFIELD TRANSFORMATIONS, SEPARATIONS, AND DECOMPOSITIONS

Figure C-1 illustrates the connections (or lack thereof) among the various options for wavefield separation (or transformation) and decomposition. Boxes (a) and (b) define the P- and S-wavefields in terms of the potentials φ and ψ (Morse and Feshbach, 1953). Calculation of the potentials involves triple integrals, which are not cost effective compared to Fourier transforms. In addition, these are rigorous for isotropic media but are not defined for anisotropic media.

Box (c) works in both isotropic and anisotropic media; boxes (b) and (c) give the same results for isotropic media. Box (c) is the most significant new conceptual step in this paper because it can be extended to anisotropic media and it provides the theoretical basis and physical interpretation (see Appendix A) for all the wavefield transformations/decompositions from boxes (d) through (i).

From box (b), we see that box (d) defines only a part of the integration kernels. The consequence is that box (d) delivers wavefield transforms (the

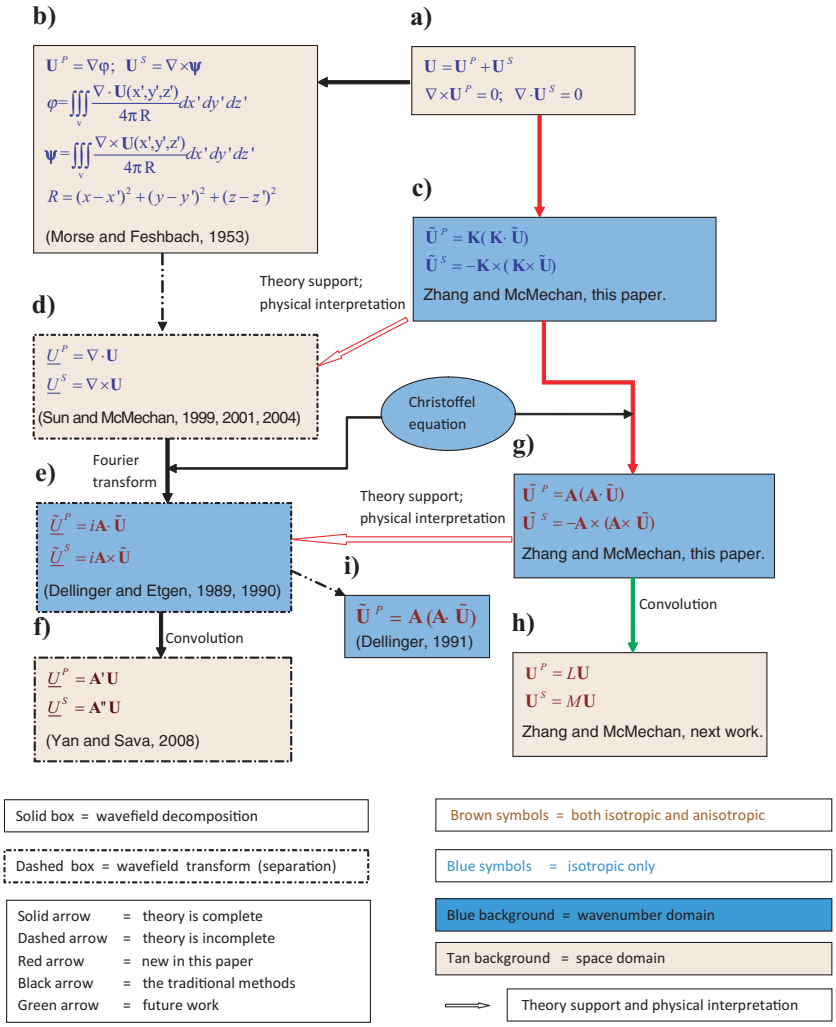

Figure C-1. Relations between wavefield separations (or transformations) on the left and decompositions on the right. The underlines in (d), (e), and (f) indicate that these wavefields are obtained by separation rather than by decomposition.

divergence and curl), but they are incomplete in terms of rigorous wavefield separation/decomposition Prior to the derivation of the operators in box (c) and Appendix A, the rationale for why box (d) works (or how to interpret it physically) was not understood. Decomposition is reversible; separation is not. Box (c) is the previously missing link, and it also provides the mathematical basis for extension to anisotropic media.

Boxes (d), (e), and (f) form a natural series whose connections are well understood. Boxes (e) and (f) are equivalent representations in the space and wavenumber domains. With the addition of the Christoffel equation, boxes (e) and (f) are applicable to anisotropic media. Similarly, boxes (c), (g), and (h) form the equivalent vector decompositions. Box (i) has the same result for P-waves as box (g) (equation 21 in the text) but has no equivalent to the second equation (for $\tilde{\mathbf{U}}^S$) in box (g) (equation 22 in the text).

In box (f), the composite operators $\mathbf{A}'$ and $\mathbf{A}''$ are as defined by Yan and Sava (2009) (compare with box (g)). In box (h), L and M are defined via the procedure of Yan and Sava (2009).

REFERENCES

Agnihotri, Y., and G. A. McMechan, 2007, Parsimonious migration of 3-C 3D VSP data: Geophysics, **72**, no. 6, S205–S213.

Aki, K., and P. G. Richards, 1980, Quantitative seismology: Theory and methods: W. H. Freeman.

Amundsen, L., L. T. Ikelle, and J. Martin, 1998, Multiple attenuation and P/S splitting of OBC data: A heterogeneous sea floor: 68th Annual International Meeting, SEG, Expanded Abstracts, 722–725.

Amundsen, L., and A. Reitan, 1995, Decomposition of multicomponent sea-floor data into upgoing and downgoing P- and S-waves: Geophysics, **60**, 563–572.

Carcione, J. M., 2007, Wave fields in real media: Wave propagation in anisotropic, anelastic, porous and electromagnetic media, 2nd ed., Handbook of geophysical exploration, v. 38: Elsevier Ltd.

Červený, V., 2001, Seismic ray theory: Cambridge University Press.

Crampin, S., 1981, A review of wave motion in anisotropic and cracked elastic media: Wave Motion, **3**, 343–391.

Crampin, S., and M. Yedlin, 1981, Shear-wave singularities of wave propagation in anisotropic media: Journal of Geophysics, **49**, 43–46.

Dellinger, J., 1991, Anisotropic seismic wave propagation: Ph.D. thesis, Stanford University; accessed January 2010, http://sepwww.stanford.edu/data/media/public/oldreports/sept69/.

Dellinger, J., and J. Etgen, 1989, Wave-type separation in 3-D anisotropic media: 59th Annual International Meeting, SEG, Expanded Abstracts, 977–979. http://dx.doi.org/10.1190/1.1889836.

———, 1990, Wave-field separation in two-dimensional anisotropic media: Geophysics, **55**, 914–919. http://dx.doi.org/10.1190/1.1442906

Devaney, A. J., and M. L. Oristaglio, 1986, A plane-wave decomposition for elastic wave fields applied to the separation of P-waves and S-waves in vector seismic data: Geophysics, **51**, 419–423.

Dieulesaint, E., and D. Royer, 1974, Elastic waves in solids: Applications to signal processing, trans. A. Bastin and M. Motz: John Wiley & Sons.

Gomes, E., X. Zheng, I. Pšenčík, S. Horne, and S. Leaney, 2004, Local determination of weak anisotropy parameters from walkaway VSP qP-wave data in the Java Sea Region: Studia Geophysica et Geodaetica, **48**, 215–231.

Jianlei, Z., T. Zhenping, and W. Chengxiang, 2007, P- and S-wave separated elastic wave equation numerical modeling using 2D staggered-grid: 77th Annual International Meeting, SEG, Expanded Abstracts, 2104–2109.

Komatitsch, D., and R. Martin, 2007, An unsplit convolutional perfectly matched layer improved at grazing incidence for the seismic wave equation: Geophysics, **72**, no. 5, SM155–SM167.

Ma, D., and G. Zhu, 2003, P- and S-wave separated elastic wave equation numerical modeling (in Chinese): Oil Geophysical Prospecting, **38**, 482–486.

Morse, P. M., and H. Feshbach, 1953, Methods of theoretical physics: McGraw-Hill Book Company.

Nistala, S., and G. A. McMechan, 2005, 3D modeling of fracture-induced shear-wave splitting in the Southern California Basin: Bulletin of the Seismological Society of America, **95**, 1090–1100.

Sava, P., and S. Fomel, 2005, Coordinate-independent angle-gathers for wave equation migration: 75th Annual International Meeting, SEG, Expanded Abstracts, 2052–2055.

Sun, R., J. Chow, and K.-J. Chen, 2001, Phase correction in separating P- and S-waves in elastic data: Geophysics, **66**, 1515–1518.

Sun, R., and G. A. McMechan, 2001, Scalar reverse-time depth migration of prestack elastic seismic data: Geophysics, **66**, 1519–1527.

Sun, R., G. A. McMechan, H.-H. Hsiao, and J. Chow, 2004, Separating P- and S-waves in prestack 3D elastic seismograms using divergence and curl: Geophysics, **69**, 286–297.

Sun, R., G. A. McMechan, C.-S. Lee, J. Chow, and C.-H. Chen, 2006, Prestack scalar reverse-time depth migration of 3D elastic seismic data: Geophysics, **71**, no. 5, S199–S207.

Tarantola, A., 1988, Theoretical background for the inversion of seismic waveforms, including elasticity and attenuation: Pure and Applied Geo

physics, **128**, no. 1–2, 365–399.
Tsvankin, I., 1997, Reflection moveout and parameter estimation for horizontal transverse isotropy: Geophysics, **62**, 614–629.
——–, 2005, Seismic signatures and analysis of reflection data in anisotropic media, 2nd ed.: Elsevier Science.
Vavryčuk, V., 2003, Behavior of rays near singularities in anisotropic media: Physical Review B, **67**, 054105-1–054105-8.
Yan, J., and P. Sava, 2007, Elastic wavefield imaging with scalar and vector potentials: 77th Annual International Meeting, SEG, Expanded Abstracts, 2150–2154.
——–, 2009, Elastic wave-mode separation for VTI media: Geophysics, **74**, no. 5, WB19–WB32.